中國機械工程學刊第四十六卷第一期第17~31頁(民國一百一十四年)
Journal of the Chinese Society of Mechanical Engineers, Vol.46, No.1, pp 17~31 (2025)

Rotor Design Optimization of the Miniature Flux Switching Motor Using a Multivariate Optimization Method

Dang-Khoa Nguyen*, **, Hua-Chih Huang* and Thi-Diem-My Le*,***

Keywords : Flux switching motor, Taguchi Optimization, Grey relation analysis, Finite element method.

ABSTRACT

The Flux Switching Motor (FSM) finds wide applications across various industrial and residential domains. Enhanced motor performance correlates directly with an increase in average torque (T_{avg}), while a rise in torque ripple (T_{ripple}) leads to heightened instability, particularly evident at higher speeds. To mitigate the impact of these factors on miniature FSM operation, this study conducted simulations and analyzed the influence of rotor geometric parameters on design model performance using analytical finite element methods via JMAG software. Weighting factors for each metric were determined utilizing the entropy method. Subsequently, a multi-objective optimization approach was implemented, employing the TOPSIS-based Grey Relational Grade (GrG-TOPSIS) comprehensive evaluation method. This approach aimed to achieve the optimal combination of process parameters. This innovative combination method marks its inaugural application in FSM rotor design. Experimental findings demonstrate consistent results, with optimal average torque and torque ripple variables measuring 368.67μNm and 16.58%, respectively. Comparative analysis between initial and optimal parameters reveals a 2.95% improvement in average torque magnitude and a 7.96% reduction in torque ripple.

Paper Received April, 2024. Revised July, 2024. Accepted August, 2024. Author for Correspondence: Hua-Chih Huang.

* *Department of Mechanical Engineering, National Kaohsiung University of Science and Technology, Kaohsiung 807618, Taiwan.*

** *Faculty of Engineering and Technology, Nong Lam University, Ho Chi Minh City 700000, Vietnam.*

*** *Faculty of Economics and Industrial Management, Can Tho University of Technology, Can Tho City 900000, Viet Nam.*

INTRODUCTION

Flux switching motors have the advantages of compactness and simple structure and are used in many different industries (Ni et al., 2016; Reichert et al., 2013). They are utilized in sectors such as home appliances (Chen et al., 2006), automotive (Sulaiman et al., 2011), and aerospace (Walter et al., 2016). Notably, FSM stands out in ultrapure applications like blood pumps, fluid pumps, and air motors due to its separate rotor and stator design (Bartholet et al., 2009), offering distinct advantages in various contexts. The basic structure of a Miniature Flux Switching Motor typically includes a rotor and a stator. The rotor, which is a rotating part, windings, and permanent magnets are not present on the rotor. The stator, on the other hand, is the stationary part comprising winding coils. This configuration allows for efficient flux switching and power generation in a compact design suitable for miniature applications.

Currently, conventional motors are permanent magnet (PM) motors with high power density and efficiency compared to other motors. PM motors are categorized into "rotor-PM motors" and "stator-PM motors" based on the placement of the PM within the motor. "Rotor-PM motors" comprise four types: surface-mounted, surface-inset, interior-radial, and interior-circumferential. Extensive discussions on the performance, structure, and control methods of these motors have been documented (Laskaris et al., 2009; Wang et al., 2011; Dutta et al., 2008; Bianchi et al., 1996). A design approach is adopted to mitigate the risk of demagnetization in FSM, where the permanent magnet poles are strategically positioned within the stator structure. This arrangement ensures that both the excitation and armature windings are housed within the motor stator. This combination also results in better thermal management of PM (Cao et al., 2012). According to Gaussens et al. (2012), the air gap excitation field in FSM can be controlled by replacing permanent magnets with concentrated field windings. A distinct FSM configuration adopts a rotor topology

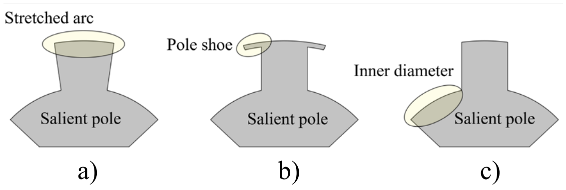

Fig. 1. Different rotor shapes affect motor performance. a) Stretched arc, b) pole shoe, c) inner diameter.

resembling the switched reluctance motor (SRM) (Mecrow et al., 2002). The resulting torque in this setup is comparable to that of SRM in the same category (Gaussens et al., 2012). FSM often exhibit higher torque ripples than other commonly used machines due to factors like high air gap flux density and interactions between electromotive force harmonics and air gap permeance harmonics. These fluctuations, transmitted via the rotor shaft to the load under dynamic conditions, can pose challenges in position and speed control. Moreover, torque ripples have the potential to induce vibration, generate acoustic noise, and trigger structural resonance within the motor stator. Specifically, in segmented rotor flux switching motors, torque ripples may escalate to levels reaching up to 50% of the average developed torque, particularly under conditions involving high armature and field currents (Lee et al., 2008).

To mitigate torque ripples in electric machines, several techniques are employed, as highlighted by Zhu et al. (2000). These methods include employing different driving strategies, implementing rotor or stator tooth shaping techniques such as fractional slot per pole (Chu et al., 2012), employing slot skewing, and optimizing notches, teeth, and pole arcs (Yang et al., 2006; Hwang et al., 2001). The shape of the rotor affects the improvement in motor performance. According to Lee et al. (2021), parameters such as the stretched arc, pole shoe, and inner diameter notably influence both average torque and torque ripple, as illustrated in Fig. 1.

Recent research has concentrated on enhancing motor architecture and control strategies to strengthen performance consistently. Pang et al. (2020) introduce the world's smallest miniature model with a soft magnetic composite core, making it easy to manufacture for micro-machine applications without the need for silicon steel lamination. With this new motor structure, topology optimization is performed on inter-pole iron widths to find the maximum torque output and reduce the torque ripple. Experiments were conducted by varying the inter-pole iron widths. Another proposal focuses on improving a new miniature motor internal Permanent Magnet Synchronous Motor (Pang et al., 2021) to enhance the torque density of micromotors. The result was achieved by optimizing the rotor shape using multiple

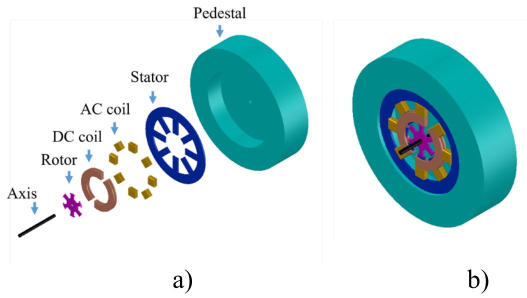

Fig. 2. a) The explosion model, b) Combination diagram of the four-phase FSM

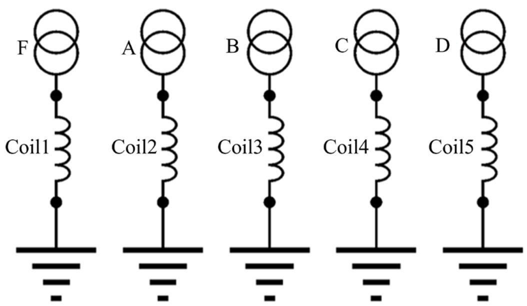

Fig. 3. Diagram circuit of the FSM

parameters to increase the magnitude of the average torque while simultaneously reducing torque ripple. By demonstrating improvements over the original model, the study contributes to the advancement of micromotor technology, potentially enabling more efficient and compact motor designs for various applications. The finite element method is used to evaluate and find the best results from the geometric parameters to improve the average moment characteristics and eliminate moment ripples proposed by Kocan et al. (2021) applied to the SRM 6/4 model. The stretched arc, inner diameter of the rotor, and parameters of the rotor and stator of the motor are selected as values to be determined to provide the optimal calculation process. Analytical results demonstrate the influence of rotor geometric parameters on output parameters such as output power, losses peak current, average torque, and torque ripple. The rotor's geometrical parameters are elements that determine the magnitude of the torque output and the torque ripple (Balaji et al., 2014). As a result, optimizing the geometric parameters of the rotor is crucial in motor design, as highlighted by reference (Naayagi et al., 2005). Specifically, optimizing parameters such as the rotor and stator pole arc can significantly impact the performance of the motor, particularly in reducing torque ripple. Balaji et al. provided a new strategy leveraging Genetic Algorithms (GA) to minimize torque dip and associated torque ripple. The proposed method aims to simultaneously reduce the size while increasing the torque output by

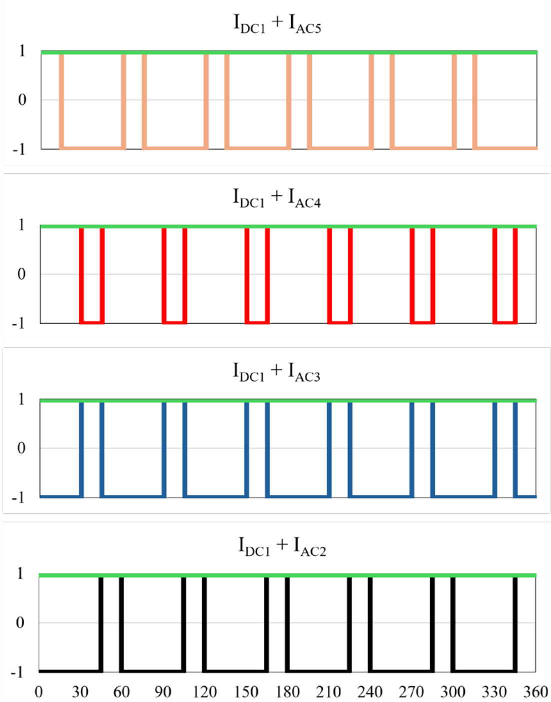

Fig. 4. Current diagram controlling FSM rotation

optimizing flux linkage and increasing torque density per unit rotor volume and inductance ratio. This finding promises the potential for combining finite element method (FEM) with optimization algorithms. By a multilevel design optimization method, Xing et al. (2016) chose the rotor tooth with the shape factors of the motor selected as initial variables. Three levels for three design variables, including the nonsensitive, mid-sensitive, and strong-sensitive levels, are analyzed. By a combination of the comprehensive sensitivity method for design goals that are nonsensitive level to small changes compared to the initial design variables and the response surface method for design goals that are mid-sensitive level for design variations, the Multi-Objective Genetic Algorithm method for targets exhibits a strong-sensitive level to the design parameters. With different methods tailored to the sensitivity of the design goals, this approach effectively achieved a design that balances the performance goals: output torque, torque ripple, and magnetic coupling. The sensitivity analysis method is used together with the genetic algorithm (Chen et al., 2019). This strategy reduced the number of optimal design variables. Four critical parameters exhibiting high sensitivity to the optimal targets are identified. By employing genetic algorithm optimization, the precision of the optimal solutions was enhanced. The results showed notable improvement, with the average output torque increasing by 28.2% and torque fluctuation decreasing by 71.8%. Omekanda et al. (2005) presented the Taguchi approach to optimize SRM

Table 1. Mechanical and electrical specification of FSM

Parameters	Value
Stator/rotor number of pole	8/6
Outer diameter of stator	25mm
Inner diameter of stator	8.6mm
Outer diameter of rotor	8mm
Inner diameter of rotor	1mm
Stator/rotor material	40CS300
Air gap	0.3mm
Thickness of motor	0.5mm
Number of winding turns	120
Current	1A
Coil resistance	0.35Ω
Arc angle of rotor and stator teeth	15 deg

for applications needing fast drives. Using the Taguchi experimental setup, the geometric parameters of the rotor and stator are selected as input variables. Univariate analysis results to find the ideal level of rotor geometric parameters. In this work, we present a new technique to increase the performance of SRM designs. Multi-Objective Genetic Particle Swarm Optimizer, as introduced by Zhang et al. (2018), is employed in motor design. The study defines objective functions, constraints, and decision variables to establish a comprehensive optimization process. Parameters such as the rotor arc, inner diameter, and other geometrical characteristics of the rotor and stator were compared with initial parameterizations based on priority calculations. FEM was employed to validate the electromagnetic performance of the optimized design. The comparative analysis demonstrated that the performance of the optimized design closely matched the FEM calculations, thus affirming the effectiveness and applicability of SRM optimization using the analytical design model. Argiolas et al. (2017) modified the form of the winding slots by adjusting other geometric characteristics and rotor tooth width to increase torque magnitude and torque ripple. The ideal result from GA raises the amplitude of the average moment while lowering its ripple.

Previous research indicates that many researchers tend to concentrate solely on investigating and refining the structural geometry of the model as topology optimization. Nevertheless, employing topology optimization for rotor mechanism modeling presents drawbacks such as extensive time and cost requirements, complexity, and restricted applicability. Additionally, acquiring

Table 2. Simulation Parameters of FSM on JMAG

Parameters	Value
Number of steps	361
End time	0.02s
Division	360
Stack length	0.5mm
Size	0.25mm

Table 3. Design variables and their levels

Factor	Symbol	Unit	Level		
			1	2	3
Pole shoe	t	mm	0.2	0.3	0.4
Stretched arc	L	mm	1.7	1.8	1.9
Inner diameter	R	mm	2	2.3	2.6

a profound comprehension of the structure and possessing the capability to conduct technical analyses pose significant challenges.

In alignment with current trends, a novel rotor structure model of the FSM was selected for research and design. Utilizing a multi-objective optimization approach, the geometric parameters of the rotor structure were thoroughly analyzed and optimized. The GrG-TOPSIS hybrid method is proposed for the first time to optimize the geometric parameters of the design, which effectively solves the optimization challenges for FSM structures. With notable advantages over topology optimization, this method is characterized by high performance and flexible evaluation capabilities, facilitating the discovery of optimal solutions with complex data and ensuring the stability and reliability of results.

The model's performance will be evaluated based on the principle of "the larger, the better" for average torque and "the smaller, the better" for torque ripple. The main geometric parameters that affect the model's performance will be carefully selected for analysis, simulation, and optimization. After thorough research and analysis, three main parameters, stretched arc, pole shoe, and inner diameter, were determined as input parameters. JMAG simulation software is a powerful and efficient tool for performing finite element simulation and analyzing FSM structures. The experimental setup encompasses L27 cases generated through the Taguchi experimental design methodology.

CONCEPTUAL DESIGN AND SIMULATION

Design model

FSM model includes the following parts: stator, rotor, and coil. The Stator has eight poles, and the rotor has six poles. The coil is wound around the

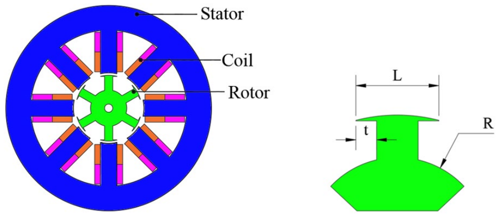

a) b)

Fig. 5. a) Drawing of FSM, b) Geometrical parameters of the rotor

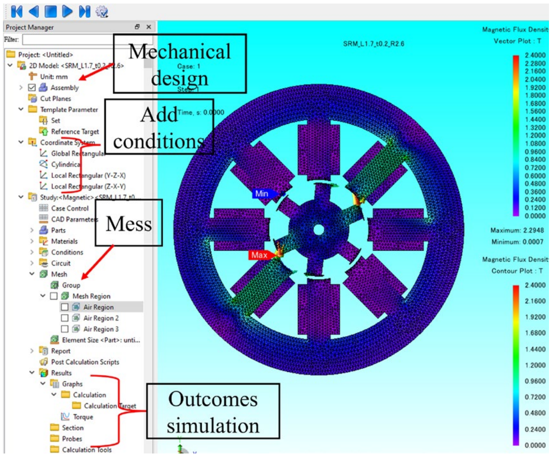

Fig. 6. FSM in JMAG software

stator, and neither the stator nor the rotor contains permanent magnets. The design parameters of the FSM design are presented in Table 1. The explosion and combination diagram of the four-phase FSM is shown in Fig. 2. FSM's winding wire consists of 5 coils. 1 DC coil (coil 1) and 4 AC coils (coil 5, 4, 3, 2). The circuit diagram of FSM is depicted in Fig. 3. The flux formation principle of FSM is explained in (Pollock et al., 2006), and the operating principle of FSM is presented in Fig. 4. The starting position of the rotor is 354° when the rotation angle of the rotor is 0°□ 15°, $I_{DC1} + I_{AC5}$, the input current of coil 5 produces magnetic flux, $I_{DC1} + I_{AC2, 3, 4}$, coils 2, 3, and 4 cancel each other, and there is no magnetic flux. When the rotor rotates at an angle of 15°□ 30°, $I_{DC1} + I_{AC4}$, the input current of coil 4 produces magnetic flux, $I_{DC1} + I_{AC2, 3, 5}$, coils 2, 3, and 5 cancel each other and do not have flux. When the rotation angle is 30°□ 45°, $I_{DC1} + I_{AC3}$, the input current of coil 3 produces magnetic flux, $I_{DC1} + I_{AC2, 4, 5}$, coils 2, 4, and 5 cancel each other, and there is no magnetic flux. Finally, when the rotation angle is 45°□ 60°, $I_{DC1} + I_{AC2}$, the input current of coil 2 produces magnetic flux, $I_{DC1} + I_{AC3, 4, 5}$, coils 3, 4, and 5 cancel each other, and there is no magnetic flux.

Table 4. Experimental results of output response to input variables using JMAG.

No.	t (Pole shoe, mm)	L (Stretched arc, mm)	R (Inner diameter, mm)	Average Torque (Tavg, µNm)	Torque ripple (Tripple, %)
1	0.2	1.7	2	366.8	20.21
2	0.2	1.7	2.3	366.4	19.87
3	0.2	1.7	2.6	364.57	19.69
4	0.2	1.8	2	366.83	26.52
5	0.2	1.8	2.3	366.33	25.97
6	0.2	1.8	2.6	363.8	25.89
7	0.2	1.9	2	366.55	19.78
8	0.2	1.9	2.3	366.52	39.4
9	0.2	1.9	2.6	356.67	38.19
10	0.3	1.7	2	365.58	18.28
11	0.3	1.7	2.3	366.00	18.21
12	0.3	1.7	2.6	361.37	18.1
13	0.3	1.8	2	368.67	16.58
14	0.3	1.8	2.3	366.26	19.97
15	0.3	1.8	2.6	364.23	19.63
16	0.3	1.9	2	360.88	20.67
17	0.3	1.9	2.3	360.07	18.23
18	0.3	1.9	2.6	358.33	34.56
19	0.4	1.7	2	358.02	19.96
20	0.4	1.7	2.3	357.79	17.9
21	0.4	1.7	2.6	356.65	17.72
22	0.4	1.8	2	363.57	16.68
23	0.4	1.8	2.3	366.62	20.27
24	0.4	1.8	2.6	361.45	16.44
25	0.4	1.9	2	356.67	17.56
26	0.4	1.9	2.3	351.25	16.89
27	0.4	1.9	2.6	355.67	22.07

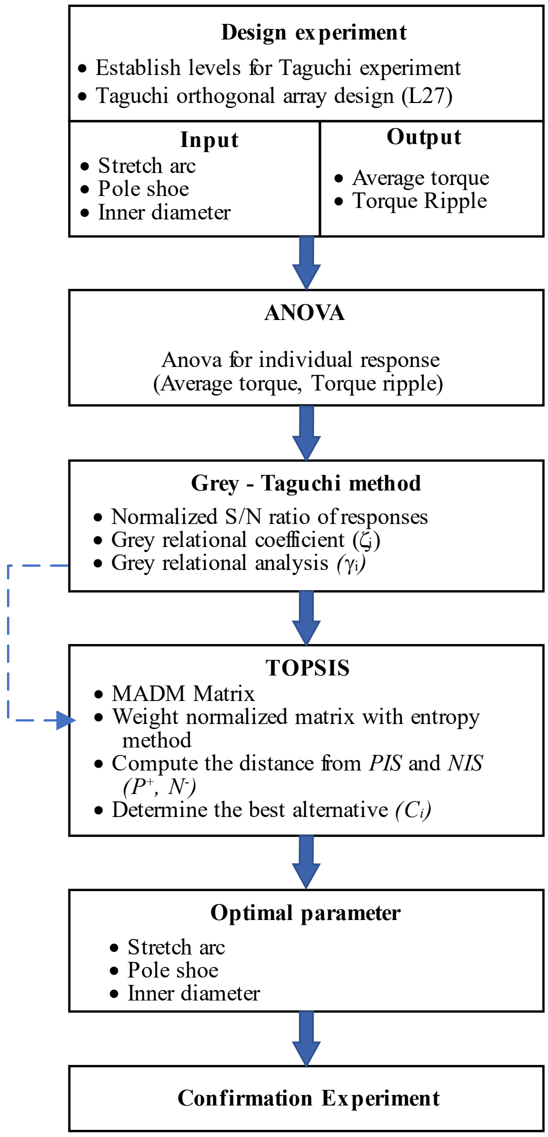

Fig. 7. GrG-TOPSIS combination diagram.

Simulation of the FSM in JMAG

After being designed directly on JMAG software, as depicted in Fig. 5, the FSM model is transferred to the simulation module to set up the necessary settings for the simulation analysis process by FEM using JMAG. The material used to simulate the stator and rotor is 50CS300 steel; the coil is copper with 120 turns and 1A excitation current. The circuit diagram was also imported into JMAG for analysis, and the winding direction of the coil was also set to generate the torque of the magnetic field. The rotor is assigned motion constraints that allow torque analysis at the output. The model was automatically meshed with element number 28544 and node number 16538. The rotor speed was set to 300 rpm and the starting position to 354 degrees. The number of simulation steps is 361, the time for each rotation is 0.2s, and the division is 360.

Validation of results includes comparing JMAG simulation results with established analytical models to ensure that the underlying physics of the FSM is accurately captured, comparing key parameters such as magnetic flux density, torque, and performance with theoretical predictions, and showing good agreement. Additionally, the simulations were compared with published data and literature to validate accuracy. Simplified models of the FSM were used to verify the accuracy of the simulation, showing consistent results with analytical solutions. Sensitivity analysis confirms robust simulation results, reinforcing confidence in predictive capabilities. A convergence study was performed by refining the mesh and ensuring the results converged to a stable solution, confirming the accuracy and reliability of the simulation results. The setup parameters and conditions are presented in Table 2. Fig. 6 shows the FSM model in JMAG software. The topic only focuses on analyzing and optimizing the geometric parameters of the rotor. The

Table 5. Table of results of objective functions and their deviations.

No.	$T_i^*(1)$	$T_i^*(2)$	$\Delta_i(1)$	$\Delta_i(2)$
1	0.8927	0.8358	0.1073	0.8927
2	0.8697	0.8506	0.1303	0.8697
3	0.7646	0.8584	0.2354	0.7646
4	0.8944	0.5610	0.1056	0.8944
5	0.8657	0.5849	0.1343	0.8657
6	0.7204	0.5884	0.2796	0.7204
7	0.8781	0.8545	0.1219	0.8781
8	0.8766	0.0000	0.1234	0.8766
9	0.3111	0.0527	0.6889	0.3111
10	0.8229	0.9199	0.1771	0.8229
11	0.8465	0.9229	0.1535	0.8465
12	0.5809	0.9277	0.4191	0.5809
13	1.0000	0.9939	0.0000	1.0000
14	0.8617	0.8463	0.1383	0.8617
15	0.7451	0.8611	0.2549	0.7451
16	0.5528	0.8158	0.4472	0.5528
17	0.5063	0.9220	0.4937	0.5063
18	0.4064	0.2108	0.5936	0.4064
19	0.3886	0.8467	0.6114	0.3886
20	0.3754	0.9364	0.6246	0.3754
21	0.3100	0.9443	0.6900	0.3100
22	0.7072	0.9895	0.2928	0.7072
23	0.8823	0.8332	0.1177	0.8823
24	0.5855	1.0000	0.4145	0.5855
25	0.3111	0.9512	0.6889	0.3111
26	0.0000	0.9804	1.0000	0.0000
27	0.2537	0.7548	0.7463	0.2537

motor control and control circuit diagram should be mentioned in this article (Pollock et al., 2006). The analysis results determine the output torque at each simulation step, with the rotor geometry parameters established. The average torque is calculated according to formula (1), and the torque ripple is calculated according to formula (2).

$$T_{avg} = \frac{\sum_{i=1}^{n} T_i}{n}, i = \{1 \ldots n\} \tag{1}$$

$$T_{ripple} = \frac{T_{\max} - T_{\min}}{T_{avg}} \times 100\% \tag{2}$$

Where n is the steps of the rotor rotation cycle, T_{max} denotes the maximum torque, T_{min} signifies the minimum torque, and T_{avg} stands for the average torque.

The input parameters are the rotor's geometric parameters, including pole shoe (t), stretched arc (L), and inner diameter (R). The level of each variable is shown in Table 3. The output parameters obtained are the average torque and torque ripple of the motor optimized to find the rotor geometric parameters: arc length, pole shoe, and internal diameter using

Table 6. Results table of GRC, GRG, and rank.

No.	$\xi_i(1)$	$\xi_i(2)$	γ_i	Rank
1	0.8233	0.7528	0.7880	6
2	0.7933	0.7700	0.7816	7
3	0.6799	0.7794	0.7296	11
4	0.8256	0.5325	0.6790	15
5	0.7882	0.5464	0.6673	16
6	0.6414	0.5485	0.5949	23
7	0.8039	0.7746	0.7893	5
8	0.8020	0.3333	0.5677	24
9	0.4206	0.3455	0.3830	27
10	0.7384	0.8619	0.8001	4
11	0.7652	0.8664	0.8158	2
12	0.5440	0.8737	0.7089	13
13	1.0000	0.9880	0.9940	1
14	0.7833	0.7648	0.7740	9
15	0.6624	0.7825	0.7225	12
16	0.5279	0.7307	0.6293	21
17	0.5032	0.8651	0.6841	14
18	0.4572	0.3878	0.4225	26
19	0.4499	0.7653	0.6076	22
20	0.4446	0.8872	0.6659	17
21	0.4202	0.8997	0.6599	19
22	0.6307	0.9795	0.8051	3
23	0.8095	0.7498	0.7797	8
24	0.5468	1.0000	0.7734	10
25	0.4206	0.9111	0.6658	18
26	0.3333	0.9623	0.6478	20
27	0.4012	0.6710	0.6332	25

TOPSIS based on GRA.

DEVELOPING A MULTI-OBJECTIVE OPTIMIZATION PROBLEM

Simulation design

The Taguchi (Freddi et al., 2018) technique was created by Dr. Genichi Taguchi, a Japanese scholar. Taguchi recommends using highly fractional factorial designs with special orthogonal arrays for designing experiments. In these designs, factors are designated as column headings, while treatment combinations are organized as rows within the orthogonal array. In this paper, the selection of the minimum number of experiments should be based on the pole shoe, stretched arc, inner diameter, and the output parameters' average torque and torque ripple.

Grey- Taguchi method

The Grey theory (Liu et al., 2012) finds wide application in systems characterized by uncertainty or lack of information, offering an effective solution to such problems with multiple discrete inputs. GRA, based on Grey theory, is recognized for its aptness in addressing multiple-factor scenarios

Table 7. Response table for S/N for GRA

Level	Factor t	Factor L	Factor R
1	-3.738	-2.790	-2.582
2	-2.955	-2.529	-3.036
3	-3.385	-4.759	-4.460
Rank	3	1	2

Table 8. Response table for means for GRA

Level	Factor t	Factor L	Factor R
1	0.665	0.7286	0.7509
2	0.728	0.7544	0.7093
3	0.682	0.5917	0.6145
Rank	3	1	2

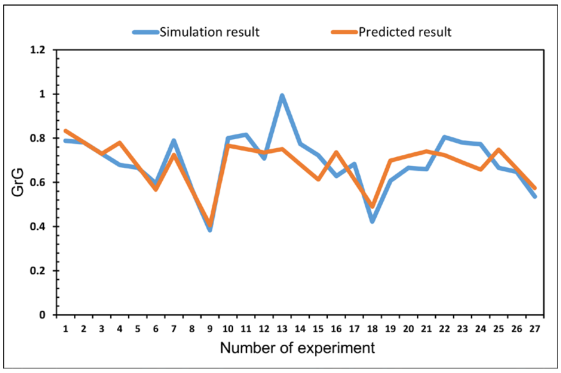

Fig. 8. The chart compares the simulated and predicted values of parameter output.

(Morán et al., 2006) and has proven useful in analyzing various Multiple Attribute Decision Making (MADM) problems (Olson et al., 2006). Initially, the task involves condensing the issue into single-property decision-making, akin to the approach employed in the TOPSIS, amalgamating all property values into a singular metric. The first phase of the GRA procedure termed grey rationalization, normalizes input values from 0 to 1 for testing data. Subsequently, in the second step, grey relation coefficients (GRC) are computed based on the normalized experimental data to elucidate the correlation between desirable and actual experimental data. Ultimately, the average GRC of selected cases is computed to ascertain the overall grey relation grade (GRG). This grade serves as an indicator of the impact performance and characteristics of parameters during the multi-response process. Using the Taguchi method's signal-to-noise (S/N) ratio, the parameter configuration with the highest GRG is then recognized as the ideal solution for the situation, allowing the quality features to be determined. Eq. (1) presents the equation for the S/N ratio:

Table 9. Analysis of variable results for GRA

ANOVA

Source	DF	Seq SS	Contribution	Adj SS	Adj MS	F-Value	P-Value
t	2	0.037	3.51%	0.037	0.018	2.160	0.177
L	2	0.355	33.96%	0.355	0.177	20.920	0.001
R	2	0.229	21.92%	0.229	0.114	13.510	0.003
t*L	4	0.142	13.64%	0.142	0.036	4.200	0.040
t*R	4	0.061	5.80%	0.061	0.015	1.790	0.225
L*R	4	0.153	14.67%	0.153	0.038	4.520	0.033
Error	8	0.068	6.49%	0.068	0.008		
Total	26	1.044	100.00%				
R-sq		93.51%					

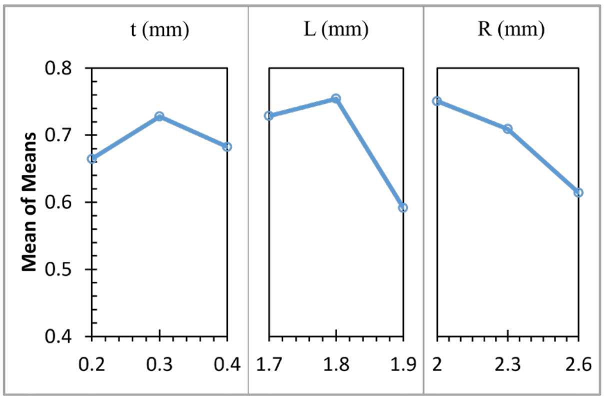

Fig. 9. Mean effects plot for means (GRA).

$$S/N = 10\log\left(\frac{1}{n}\sum_{i=1}^{n} y_i^2\right) \quad (3)$$

Step 1: Selection of design variables and their levels.
Step 2: Design experiments using orthogonal arrays (L27)
Step 3: Analyze the motor design results using rotor geometry parameters.
Step 4: Application of GRA for Rotor Variable Optimization: the rotor geometric parameters' average moment and torque ripple. With this technique, the objective function is expressed as follows:
The output value is the maximum:

$$T_i^*(k) = \frac{T_i^0(k) - \min T_i^0(k)}{\max T_i^0(k) - \min T_i^0(k)} \quad (4)$$

The output value is the minimum:

$$T_i^*(k) = \frac{\max T_i^0(k) - T_i^0(k)}{\max T_i^0(k) - \min T_i^0(k)} \quad (5)$$

The formula for calculating the deviation $\Delta_i(k)$ is as follows:

$$\Delta_{0i}(k) = \left\| T_0^*(k) - T_i^*(k) \right\| \quad (6)$$

Table 10. The result of matrix Y, YR, V

No.	Matrix Y (GRC)		Matrix YR		Matrix V	
	T_{avg}	T_{ripple}	T_{avg}	T_{ripple}	T_{avg}	T_{ripple}
1	0.9955	0.4560	0.2423	0.1867	0.1211	0.0934
2	0.4701	0.6489	0.2334	0.1910	0.1167	0.0955
3	0.3333	0.9650	0.2001	0.1933	0.1001	0.0967
4	0.9909	0.3476	0.2430	0.1321	0.1215	0.0660
5	0.4858	0.5844	0.2320	0.1355	0.1160	0.0678
6	0.3434	1.0000	0.1887	0.1360	0.0944	0.0680
7	0.9370	0.4637	0.2366	0.1921	0.1183	0.0961
8	0.4884	0.6052	0.2360	0.0827	0.1180	0.0413
9	0.3478	0.4785	0.1238	0.0857	0.0619	0.0428
10	1.0000	0.4459	0.2173	0.2138	0.1087	0.1069
11	0.4866	0.6151	0.2252	0.2149	0.1126	0.1074
12	0.3436	0.7630	0.1601	0.2167	0.0801	0.1083
13	0.9929	0.3996	0.2943	0.2451	0.1471	0.1225
14	0.5028	0.4959	0.2305	0.1897	0.1153	0.0948
15	0.3543	0.7055	0.1949	0.1941	0.0975	0.0970
16	0.9380	0.4306	0.1553	0.1813	0.0777	0.0906
17	0.5050	0.5622	0.1481	0.2146	0.0740	0.1073
18	0.3589	0.5689	0.1345	0.0962	0.0673	0.0481
19	0.9721	0.3333	0.1324	0.1898	0.0662	0.0949
20	0.4970	0.4423	0.1308	0.2201	0.0654	0.1100
21	0.3524	0.8169	0.1236	0.2232	0.0618	0.1116
22	0.9630	0.4533	0.1856	0.2430	0.0928	0.1215
23	0.5127	0.4974	0.2382	0.1860	0.1191	0.0930
24	0.3632	0.8385	0.1609	0.2480	0.0805	0.1240
25	0.9126	0.3413	0.1238	0.2260	0.0619	0.1130
26	0.5144	0.4564	0.0981	0.2387	0.0490	0.1193
27	0.3679	0.5461	0.1181	0.1664	0.0590	0.0832

$$\Delta_{\min} = \min_{\forall j \in i} \min_{\forall k} \left\| T_0^*(k) - T_i^*(k) \right\| \tag{7}$$

$$\Delta_{\max} = \max_{\forall j \in i} \max_{\forall k} \left\| T_0^*(k) - T_i^*(k) \right\| \tag{8}$$

The initial simulation results of the two-output feedback, namely T_{avg} and T_{ripple} of the FSM, are considered raw data. Data normalization steps are calculated using Eqs. (4-5) from initial data to prevent data distortion. In this work, the target function of average torque is "larger – the better," and torque ripple is ''smaller - the better'':

The GRC ξ_i was calculated and established as follows:

$$\zeta_i(k) = \frac{\Delta_{\min} + \zeta\Delta_{\max}}{\Delta_{0i}(k) + \zeta\Delta_{\max}} (0 \le \zeta_i \le 1) \tag{9}$$

The commonly used distinguishing coefficient ζ is 0.5.

The entropy method is chosen to determine weights for the TOPSIS method due to its objective, data-driven nature, its ability to handle data quality issues, its capability to reduce redundancy and correlation among criteria, its seamless integration with TOPSIS requirements, and its transparency and reproducibility in decision-making. Together, these attributes ensure that the weight determination process is robust, accurate, and aligned with the goals of optimizing decision outcomes in various practical applications. The entropy method objectively determines indicator weights, ensuring that the final optimization results for FSM rotor design are balanced, data-driven, and focused on the most critical factors. The process of determining weights using the entropy method from Eqs. (10) - (15). The weight assigned to each variable was determined using the mapping function in entropy measurement, as described in the reference (Wen et al., 1998):

Table 11. Proximity coefficient values and alternative rankings.

No.	P_i^+	N_i^-	C_i	Rank
1	0.0402	0.0889	0.6886	3
2	0.0417	0.0867	0.6751	7
3	0.0545	0.0752	0.5801	10
4	0.0634	0.0765	0.5469	13
5	0.0643	0.0720	0.5281	14
6	0.0769	0.0526	0.4060	23
7	0.0402	0.0883	0.6872	4
8	0.0877	0.0690	0.4403	21
9	0.1177	0.0129	0.0989	27
10	0.0421	0.0886	0.6777	5
11	0.0383	0.0917	0.7053	2
12	0.0689	0.0738	0.5173	15
13	0.0015	0.1273	0.9884	1
14	0.0432	0.0851	0.6633	8
15	0.0565	0.0738	0.5663	12
16	0.0771	0.0570	0.4251	22
17	0.0750	0.0705	0.4846	16
18	0.1102	0.0194	0.1500	26
19	0.0860	0.0563	0.3954	24
20	0.0829	0.0706	0.4599	17
21	0.0862	0.0714	0.4529	19
22	0.0544	0.0913	0.6266	9
23	0.0418	0.0870	0.6755	6
24	0.0667	0.0884	0.5701	11
25	0.0860	0.0728	0.4585	18
26	0.0982	0.0780	0.4426	20
27	0.0971	0.0430	0.3071	25

$$\omega_e(\rho_i) = \rho_i * e^{(1-\rho_i)} + (1-\rho_i) * e^{\rho_i} - 1 \tag{10}$$

Where $\omega_e(\rho_i)$ is the mapping function of the entropy algorithm, and $\rho_i = \frac{T_i(k)}{T_k}$

The sum of GRC (T_k) obtained by Eq. (11)

$$T_k = \sum_{i=1}^{m} T_i(k) \tag{11}$$

Calculate the normalization coefficient K:

$$K = \frac{1}{e^{0.5} - 1} = \frac{1}{0.6478 * m}$$

Where m is the number of attributes.

From Eq. (10), the entropy e_k is calculated by Eq.:

Table 12. Response table for S/N ratios for GrG-TOPSIS

Level	Factor		
	t	L	R
1	-6.719	-5.023	-4.616
2	-5.661	-4.397	-5.134
3	-6.46	-9.42	-9.09
Rank	3	1	2

Table 13. Response table for mean for GrG-TOPSIS

Level	Factor		
	t	L	R
1	0.5168	0.5725	0.6105
2	0.5753	0.619	0.5639
3	0.4876	0.3883	0.4054
Rank	3	1	2

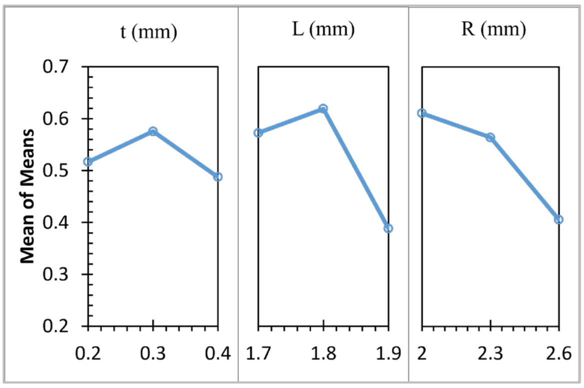

Fig. 10. Mean effects plot for means (GrG-TOPSIS)

$$e_k = K\sum_{i=1}^{m} \omega_e(\rho_i) \quad (12)$$

Here, $\omega_e(\rho_i)$ uses Eq. (10)

Eq. (13) calculates the sum of entropy:

$$E = \sum_{k=1}^{n} e_k \quad (13)$$

The relative weighting factor was calculated by Eq. (14)

$$\beta_k = \frac{1}{n-E}.(1-e_k) \quad (14)$$

w_k is the normalized weight of each attribute, which can be determined as follows:

$$w_k = \frac{\beta_k}{\sum_{k=1}^{n}\beta_k} \quad (15)$$

The mean value of GRC, GRG is computed as follows:

$$\gamma_i = \frac{\sum_{k=1}^{n} w_k \xi_i(k)}{\sum_{k=1}^{n} w_k} \quad (16)$$

TOPSIS method

The TOPSIS method, as referenced in (Lai et al., 1994), has the advantage of computational simplicity and logic. It enables rapid determination of the best solution to multiple-criteria-decision matrix (MC-DMs) problems from a finite set of potential solutions, as highlighted in (Hwang et al., 1981; Balaji et al., 2018; Nguyen et al., 2018; Du et al., 2022; Trung et al., 2021). This study's TOPSIS method is constructed based on the grey coefficient. The interpretation of the TOPSIS method relies on the following formulas, as described in (Rana et al., 2021; Tran et al., 2021; Chen et al., 2022):

Step 1: The decision Y-Matrix is created by Eq. (17):

$$Y = \left(y_{ij}\right)_{mxn} = \begin{bmatrix} y_{11} & y_{12} & \cdots & y_{1n} \\ y_{21} & y_{22} & \cdots & y_{2n} \\ \cdots & \cdots & \cdots & \cdots \\ y_{m1} & y_{m2} & \cdots & y_{mn} \end{bmatrix} \quad (17)$$

Where n represents the quantity of output response variables, while denotes the values extracted from GRC, from the decision matrix Y-Matrix, the normalization matrix *YR* is constructed as follows:

$$YR = \left(yr_{ij}\right)_{mxn} = \begin{bmatrix} yr_{11} & yr_{12} & \cdots & yr_{1n} \\ yr_{21} & yr_{22} & \cdots & yr_{2n} \\ \cdots & \cdots & \cdots & \cdots \\ yr_{m1} & yr_{m2} & \cdots & yr_{mn} \end{bmatrix} \quad (18)$$

Where:

$$\left(yr_{ij}\right)_{mxn} = \frac{y_{ij}}{\sqrt{\sum_{i=1}^{m} y_{ij}^2}}, i \in \{1,2,...,m\}, j \in \{1,2,...,n\} \quad (19)$$

Step 2: The weights are normalized as follows:

$$V = \left(w_j yr_{ij}\right)_{mxn} \quad (20)$$

w_j is calculated by Eqs. (10) – (12).

Step 3: The positive ideal *(PIS, V^+)* and negative ideal *(NIS, V^-)* are determined by the following Eqs.:

$$V^+ = \left\{v_1^+, v_2^+, v_3^+, ..., v_n^+\right\}, v_j^+ = \max_{1\le i\le m}\left\{v_{ij}\right\}, j \in N \quad (21)$$

$$V^- = \left\{v_1^-, v_2^-, v_3^-, ..., v_n^-\right\}, z_j^- = \min_{1\le i\le m}\left\{v_{ij}\right\}, j \in N$$

Table 14. Analysis of variable result for GrG-TOPSIS

ANOVA							
Source	DF	Seq SS	Contribution	Adj SS	Adj MS	F-Value	P-Value
t	2	0.036	4.24%	0.036	0.018	2	0.197
L	2	0.268	31.70%	0.268	0.134	14.95	0.002
R	2	0.208	24.60%	0.208	0.104	11.6	0.004
t*L	4	0.144	17.07%	0.144	0.036	4.03	0.045
t*R	4	0.054	6.43%	0.054	0.014	1.52	0.285
L*R	4	0.063	7.47%	0.063	0.016	1.76	0.229
Error	8	0.072	8.48%	0.072	0.009		
Total	26	0.846	100%				
R-sq	91.52%						

(22)

Step 4: The separation measure is calculated using equations (20) – (22) as follows:

$$P_i^+ = \sqrt{\sum_{j=1}^{n}\left(v_{ij} - v_j^+\right)^2}, i = \{1, 2, 3..., m\} \tag{23}$$

$$N_i^- = \sqrt{\sum_{j=1}^{n}\left(v_{ij} - v_j^-\right)^2}, i = \{1, 2, 3..., m\} \tag{24}$$

Step 5: The relative closeness C_i is the optimal calculated as follows:

$$C_i = \frac{N^-}{P_i^+ + N_i^-}, i = \{1, 2, ..., m\} \tag{25}$$

Integrate GrG -TOPSIS method

The hybrid optimization approach provides a streamlined workflow for processing data, effectively reducing processing time while offering consumers a more efficient way to pick ideal criteria. In previous studies, Zhang et al. (2019) used this method to solve the decision-making problem in fuzzy approximate space, applying the TOPSIS method. Fuzzy operators are combined with fuzzy sets. The two sets of fuzzy coarse-grained models are then analyzed, focusing on their overlap, essential properties, and classifications. Finally, an improved method to calculate target weights using fuzzy coarse models is built on the first overlay. To tackle the issue of the material problem, Vahdani et al. (2011) utilized fuzzy rough set theory to deal with uncertain data. They also used TOPSIS to determine objective criteria weights. Combining these two approaches, they proposed a new way of generating decisions based on many criteria. The combination of fuzzy and TOPSIS approaches has been thoroughly researched and widely accepted as a dependable tool for decision-making in different applications, such as robot selection and rapid prototyping in production settings. The TOPSIS is an effective ranking methodology that efficiently identifies the best answer. It uses grey coefficients to generate a decision-making matrix, which helps evaluate the range of data and facilitates the evaluation process. Optimizing the design of FSM rotors requires robust, reliable, and efficient multi-criteria decision-making (MCDM) methods. GRG and TOPSIS are two MCDM techniques well-suited for such tasks, especially in scenarios involving multiple conflicting criteria and incomplete information. GRG is effective in handling uncertain or incomplete data, simple to implement, computationally efficient, and robust in evaluating multiple criteria. These qualities make it ideal for optimizing FSM rotor designs, where parameters and performance metrics may not always be precisely known. TOPSIS is conceptually simple, ensures effective normalization of criteria, and provides clear rankings of alternatives, facilitating practical and efficient decision-making in FSM rotor design. Compared to other techniques like the Analytic Hierarchy Process (AHP), GA, Particle Swarm Optimization (PSO), and Fuzzy Logic, GRG and TOPSIS offer a balanced and straightforward approach, avoiding excessive complexity and computational demands. This study highlights the reliability and effectiveness of GRG and TOPSIS in optimizing FSM rotor designs, leading to improved performance, energy efficiency, smooth motor operation, and user experience. Fig. 7 shows the process of computation.

RESULT AND DISCUSSION

Experiment design

This study observes the impact of the geometric parameters of the rotor profile, namely shoe pole (t), stretched arc (L), and inner diameter (R), on the output factors average Torque and Torque ripple. Simulation results show output instability when changing input factors. The GRA optimization algorithm draws its foundation from the principles of the Taguchi method to find the input variables that give the output response the largest T_{avg} and the smallest T_{ripple}. In this study, the Taguchi method is used to establish the orthogonal array for the optimization process. To analyze the elements comprehensively and understand their interactions, which is essential for optimizing engine performance, an $L_{27}(3^{\wedge 3})$ orthogonal array (Dhanalakshmi, S., et al., 2018) of 27 rows is chosen for the three primary elements: pole shoe (t), stretched arc (L), and inner diameter (R). The orthogonal array is chosen based on three factors in the following order: the number of elements and their interactions, the number of element levels, and desired resolution or cost constraints. Choosing L27 for analysis is performed more comprehensively and accurately. Minitab 21 software is used to support simulation. The input variables and their levels are given in Table 3. The observed responses include the average torque and torque ripple. Experimental results of output response to input variables using JMAG are provided in Table 4.

Multivariate optimization

GRG calculation results

Initially, the original data values are normalized to the range [0-1], where higher values for the average torque response indicate better performance, while smaller values indicate better performance for torque ripple. The normalization of data results is accomplished using Eqs. (4) and (5). Subsequently, the deviation series is calculated through Eqs. (6)-(8), determine the deviations $\Delta_i(k)$. The resultant calculations are displayed in Table 5. Following this, the discrimination coefficient is utilized to adjust the comparison environment's range, replacing the GRC in Eq. (9) with ζ set at 0.5. The final step involves determining the grey relation level coefficient, based on Eq. (16), with the coefficients identified and illustrated in Table 6. Furthermore, this work determines the weight using the entropy method (Eq. 10), resulting in weights of 0.50003 and 0.49997, respectively.

A larger GRG indicates higher output efficiency. As depicted in Table 6 and Fig. 8, the best experimental performance among the 27 results is the 13th experiment, with the largest GRG value of 0.9940. In Experiment 13, the rotor's geometric parameters were a stretched arc of 1.8mm, pole shoe of 0.3mm, and inner diameter of 2mm, resulting in an average torque of 368.67 µNm and torque ripple of 16.58%. The calculation results are further analyzed for parameters (t, L, R) by calculation and analysis signal to noise (S/N). The optimal configuration for the rotor geometrical parameters is $t_2L_2R_1$, as detailed in Table 7. To be able to more clearly determine the evaluation effectiveness of each parameter. Fig. 9 shows the Main Effects Plot for the mean value of GRG to graphically evaluate the input parameters. Analyzing the interaction and main effects plots, parameters such as pole shoe, stretched arc, and inner diameter exhibit significance at levels t_2, L_2, and R_1. Conversely, the remaining parameters demonstrate negligible impact on the average torque magnitude and torque fluctuation. Significantly, the stretched arc parameter demonstrates the most substantial influence on the output response, as indicated by the maximum deviation calculated from the difference between the highest and lowest values in the plot. This notable difference underscores the more significant impact of this parameter compared to others. Means GRG values are provided in Table 8. The optimal parameter combination is chosen based on higher average GRG values, indicating that the most effective combination to maximize performance includes a pole shoe of 0.3mm, a stretched arc of 1.8mm, and an inner diameter of 2mm.

Table 15. Comparison table of evaluation results

	Initial Parameter	Optimal Parameter			
		GRA		GrG - TOPSIS	
		Prediction	Optimal test	Prediction	Optimal test
Level	$t_3L_1R_2$	$t_2L_2R_1$	$t_2L_2R_1$	$t_2L_2R_1$	$t_2L_2R_1$
Pole shoe (t, mm)	0.4	0.3	0.3	0.3	0.3
Stretched arc (L, mm)	1.7	1.8	1.8	1.8	1.8
Inner diameter (R, mm)	2.3	2.0	2.0	2.0	2.0
GRG	0.666	0.850	0.994		
C_i	0.4599			0.752	0.9884
Improvement		0.184	0.328	0.2921	0.5285

The results of ANOVA analysis for the characteristics are shown in Table 9 with a confidence level of 0.95 and a significance level of 0.05. According to Table 9, the stretched arc and inner diameter of the rotor are notable factors, and there is a significant interaction between the stretched arc and inner diameter. Specifically, the stretched arc contributes the most, with a ratio of 33.96% to the motor output. Additionally, the inner diameter and pole shoes contribute 21.92% and 3.51%, respectively, to the variance. Evaluation is based on priority output criteria. Therefore, the change in the length of the stretched arc will be the most significant factor affecting the output torque. The coefficient of determination R^2 is calculated as 93.51%, indicating this linear regression model's adequacy for explaining the data's variability.

GrG-TOPSIS combination method result

GRA analysis results from selected input variables that influence output parameters the most. The GRC value from the GRA analysis is placed into the decision matrix *Y*. The matrix *YR* is normalized from the matrix *Y* using Eqs. (17) and (18). Eq. (19) calculates the elements in the *YR* matrix, which are also the benefit attributes, in which the values of two attributes are inversely proportional to each other, meaning that as one attribute increases, the other decreases with the same level of change. This study utilized the benefit attribute, with attribute weights specified using the entropy method through Eqs. (10)-(12) sequentially, as depicted in Table 10. The values in matrix *V* are calculated using Eq. (20). After calculating the *V* matrix, the positive and negative roots are computed using the Eqs. (21) and (22). Eqs. (23) and (24) are used to calculate the nearest and farthest alternatives *(PIS, NIS)*. The closest coefficient is calculated using Eq. (25). Finally, the

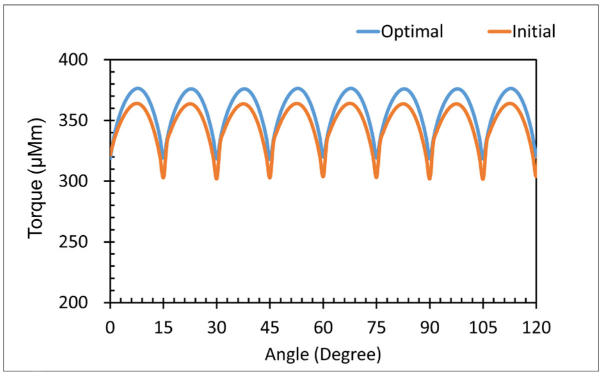

Fig.11. Torque – Angle curve for each step between initial parameter and optimal parameter.

optimal calculation result is selected based on the value of C_i, the best choice with the largest Ci result, as shown in Table 11. Notably, experiment 13 shows the coefficient close to the highest, indicating its closeness to the ideal case. Table 12 shows the results of the S/N ratio analysis for GrG-TOPSIS; the maximum value of the input parameters is the optimal result. Through analysis of Table 12, $t_2L_2R_1$ is the optimal result with a pole shoe of 0.3mm, stretched arc of 1.8mm, and inner diameter of 2.0mm. The results of the analysis of the means are presented in Table 13, and the optimal results are agreed upon compared to the results of the analysis of the S/N ratio. The graphical optimization analysis method also gives similar results, as shown in Fig. 10.

Additionally, ANOVA output for multiple performance characteristics is provided in Table 14. Notably, the stretched arc and inner diameter of the rotor emerge as remarkable factors, with the stretched arc contributing the most at 31.70%. Consequently, the stretched arc significantly impacts the output parameter based on the preferred configuration output. The inner diameter and pole shoe contributions were 24.60% and 4.24%, respectively. Although pole shoes (t) have the lowest contribution rate compared to the remaining factors, they have a significant contribution rate when considering the level of interaction with the remaining factors. The contribution rate of pole shoe and stretched arc (t*L) is 17.07%, the highest among the remaining interaction pairs. Furthermore, the coefficient of determination R^2 is calculated as 91.52%, indicating the suitability of this linear regression model for explaining 91.52% of the dataset.

SIMULATION TEST AND COMPARE THE OUTPUT RESULTS

A verification test was conducted to assess the quality of the response output. The predicted optimal value was calculated using Eq. (26).

$$\eta_{predict} = \eta_{tm} + \sum_{i=1}^{t}(\eta_i - \eta_{tm}) \tag{26}$$

Where η_{tm} is the overall mean value of the response, η_i is the mean of the response at the best level, and t is the number of parameter inputs. The result of the confirmatory experiment is shown in Table 15.

In Table 15, the basic specifications from the design requirement were a pole shoe of 0.3mm, a stretched arc of 1.8mm, and an inner diameter of 2.0mm. The ideal parameters, estimated by both GRA and Grey-TOPSIS techniques, were the same: an inner diameter of 2.0mm, a stretched arc of 1.8mm, and a pole shoe of 0.3mm. However, the investigation suggested that the valuation coefficient, according to the GrG-TOPSIS approach, improved more than the GRA method. It is interesting that the quality responsiveness of displacement is enhanced by utilizing this proposed strategy. The improvement is the result of advanced design techniques using the GrG -TOPSIS hybrid optimization algorithm applied for the first time on FSM. With the advantages of high performance and flexible evaluation capabilities, it facilitates the discovery of optimal solutions with complex data and ensures the stability and reliability of results. Input factors are analyzed more comprehensively and accurately based on the L27 orthogonal array. This combination allows the motor design to be explored with different rotor design configurations to maximize torque and minimize ripple. The maximum output torque is 368.67μNm, with a torque ripple of 16.58%. The comparison between the initial and optimal parameters shows that the average torque magnitude is improved by 2.95%, and the torque ripple is increased by 7.96%. These enhancements help improve engine performance to increase energy savings and reduce operating costs, improving reliability and longevity. The engine operates smoother and quieter, increasing the user experience. A graph comparing the output torque between the optimal parameters and the initial parameters simulated by JMAG is provided in Fig. 11.

CONCLUSION

This article introduces a method for determining the optimal geometric parameters for the rotor of an FSM using a multi-object optimization approach. Initially, a model was designed, and simulation analysis was conducted using FEM through JMAG software for FSM. Subsequently, a test set consisting of 27 experiments was established using the experimental layout method, according to Taguchi. The results of ANOVA were employed to assess the significance and contribution of parameters such as stretched arc, pole shoe, and inner diameter on average torque and torque ripple.

This study proposes a novel integrated method combining GrG - TOPSIS and entropy weighting calculation to determine the optimal values of geometric parameters for the rotor, aiming to maximize T_{avg} and minimize T_{ripple}. The proposed optimization method applies not only to rotor design but also to other complex multivariate optimization problems.

Optimal results were achieved with the following design parameters: a pole shoe (t) of 0.3 mm, a stretched arc (L) of 1.8 mm, and an inner diameter (R) of 2.0 mm. The maximum output torque is 368.67μNm, with a torque ripple of 16.58%. Comparison between the initial and optimal parameters reveals a 2.95% improvement in average moment magnitude and a 7.96% enhancement in torque ripple. The increase in torque improves motor performance, enables energy savings, and enhances the ability to handle heavy loads in industrial settings. The reduction in torque ripple leads to more stable motor operation, reducing noise and vibration, which is crucial for applications requiring precise speed control. These improvements are significant in fields such as automotive, industrial machinery, and renewable energy, resulting in increased efficiency, energy savings, and improved reliability.

In the future, we plan to proceed with manufacturing a prototype of the FSM based on the optimized design from the JMAG simulation and then conduct experiments to measure key performance indicators such as torque torsion, efficiency, thermal performance, and electromagnetic behavior. The prototype model will be combined with various control and monitoring methods to achieve better results.

REFERENCES

Argiolas, O., Nazeraj, E., Hegazy, O., Backer, J. D., Mohammad, A., and Mierlo, J. V., "Design optimization of a 12/8 Switched Reluctance Motor for electric and hybrid vehicles," in *2017 Twelfth International Conference on Ecological Vehicles and Renewable Energies (EVER)*, pp. 1-10, (2017).

Balaji, M., Ramkumar, S., and Kamaraj, V., "Sensitivity Analysis of Geometrical Parameters of a Switched Reluctance Motor with Modified Pole Shapes," *Journal of Electrical Engineering and Technology,* vol. 9, no. 1, pp. 136-142, (2014).

Balaji, V., Ravi, S., and Chandran, P. N., "Optimization on cryogenic Co2 machining parameters of AISI D2 steel using Taguchi based grey relational approach and TOPSIS," *Int J Eng Technol,* vol. 7, no. 3.12, p. 885, (2018).

Bartholet, M. T., Nussbaumer, T., Silber S., and Kolar, J. W., "Comparative evaluation of polyphase bearingless slice motors for fluid-handling applications," IEEE Transactions on Industry Applications, vol. 45, no. 5, pp. 1821-1830 (2009).

Bianchi, N., Bolognani, S., and Zigliotto, M., "Analysis of PM synchronous motor drive failures during flux weakening operation," in PESC Record. 27th Annual IEEE Power Electronics Specialists Conference, vol. 2: IEEE, pp. 1542-1548 (1996).

Cao, R., Mi, C., and Cheng, M., "Quantitative comparison of flux-switching permanent-magnet motors with interior permanent magnet motor for EV, HEV, and PHEV applications," IEEE Transactions on Magnetics, vol. 48, no. 8, pp. 2374-2384 (2012).

Chen, H., "Power parametric optimization of an electro-hydraulic integrated drive system for power-carrying vehicles based on the Taguchi method," *Processes,* vol. 10, no. 5, p. 867, (2022).

Chen, Y., Chen, S., Zhu, Z., Howe, D., and Ye, Y., "Starting torque of single-phase flux-switching permanent magnet motors," IEEE Transactions on Magnetics, vol. 42, no. 10, pp. 3416-3418 (2006).

Chen, Y., Zhuang, J., Ding, Y., and Li, X., "Optimal Design and Performance Analysis of Double Stator Multi Excitation Flux Switching Machine," *IEEE Transactions on Applied Superconductivity,* vol. 29, no. 2, pp. 1-5, (2019).

Chu, W. and Zhu, Z., "Investigation of torque ripples in permanent magnet synchronous machines with skewing," IEEE Transactions on Magnetics, vol. 49, no. 3, pp. 1211-1220 (2012).

Dhanalakshmi, S., Mohanasundararaju, N., Venkatakrishnan, P. G., and Karthik, V. "Optimization of friction and wear behavior of Al7075-Al2O3-B4C metal matrix composites using Taguchi method." *IOP Conference Series: Materials Science and Engineering*, Vol. 314. No. 1. p. 012025, (2018).

Du, Y., Zhou, Z., He, G., and Xu, L., "Multi-parameter optimization of laser cladding 15-5PH Using TOPSIS-GRA based on combined weighting method," *Journal of Materials Engineering and Performance,* pp. 1-15, (2022).

Dutta, R., and Rahman, M., "Design and analysis of an interior permanent magnet (IPM) machine with very wide constant power operation range," IEEE Transactions on Energy Conversion, vol. 23, no. 1, pp. 25-33 (2008).

Freddi, A., and Salmon, M., "Design principles and methodologies: From conceptualization to first prototyping with examples and case studies," Springer, (2018).

Gaussens, B., "Analytical armature reaction field prediction in field-excited flux-switching machines using an exact relative permeance function," IEEE Transactions on Magnetics, vol. 49, no. 1, pp. 628-641 (2012)

Hwang, C. L., Yoon, K., Hwang, C. L., and Yoon, K., "Methods for multiple attribute decision making," *Multiple attribute decision making: methods and applications a state-of-the-art survey,* pp. 58-191, (1981).

Hwang, S. M., Eom, J. B., Jung, Y. H., Lee, D. W., and Kang, B. S., "Various design techniques to reduce cogging torque by controlling energy variation in permanent magnet motors," IEEE Transactions on Magnetics, vol. 37, no. 4, pp. 2806-2809 (2001).

Kocan, S., Rafajdus, P., Bastovansky, R., Lenhard, R., and Stano, M., "Design and Optimization of a High-Speed Switched Reluctance Motor," *Energies,* vol. 14, no. 20, (2021).

Lai, Y. J., Liu, T. Y., and Hwang, C. L., "Topsis for MODM," *European Journal of Operational Research,* vol. 76, no. 3, pp. 486-500, (1994).

Laskaris, K. I., and Kladas, A. G., "Internal permanent magnet motor design for electric vehicle drive," IEEE Transactions on Industrial Electronics, vol. 57, no. 1, pp. 138-145 (2009).

Lee, C., Lee, J., and Jang, I. G., "Shape optimization-based design investigation of the switched reluctance motors regarding the target torque and current limitation," *Structural and Multidisciplinary Optimization,* vol. 64, no. 2, pp. 859-870, (2021).

Lee, G. H., Kim, S. I., Hong, J. P., and Bahn, J. H., "Torque ripple reduction of interior permanent magnet synchronous motor using harmonic injected current," IEEE Transactions on Magnetics, vol. 44, no. 6, pp. 1582-1585 (2008).

Liu, S., Forrest, J., and Yang, Y., "A brief introduction to grey systems theory," *Grey Systems: Theory and Application,* vol. 2, no. 2, pp. 89-104, (2012).

Mecrow, B., Finch, J., Kharashi, E., and Jack, A., "Switched reluctance motors with segmental rotors," IEE Proceedings-Electric Power Applications, vol. 149, no. 4, pp. 245-254, (2002)

Morán, J., Granada, Míguez, E., J., and Porteiro, J., "Use of grey relational analysis to assess and optimize small biomass boilers," *Fuel processing technology,* vol. 87, no. 2, pp. 123-127, (2006).

Naayagi, R. T., and Kamaraj, V., "Modeling and design of shape optimized SRM with reduced ripple," *Proceedings of the IEEE Symposium on Emerging Technologies,* Pakistan, Islamabad, pp. 399-404, (2005).

Nguyen, P., Banh, L., Bui, V., and Hoang, D., "Multi-response optimization of process parameters for powder mixed electro-discharge machining according to the surface roughness and surface micro-hardness using Taguchi-TOPSIS," *International Journal of Data and Network Science,* vol. 2, no. 4, pp. 109-119, (2018).

Ni, X. W., Ding, Q., Wang, Y., and Deng, Z., "Novel structure of bearingless flux-switching motor for improvement of levitation force characteristics," IEEE 8th IPEMC-ECCE Asia, Hefei, pp. 1929-1933 (2016).

Olson, D. L. and Wu, D., "Simulation of fuzzy multiattribute models for grey relationships," *European Journal of Operational Research,* vol. 175, no. 1, pp. 111-120, (2006).

Omekanda, A. M., "Robust torque-and torque-per-inertia optimization of a switched reluctance motor using the Taguchi methods," in *IEEE International Conference on Electric Machines and Drives*, pp. 521-526, (2005).

Pang, D. C., Shi, Z. J., Chang, Y. H., Huang, H. C., and Bui, G. T., "Investigation of an Interior Micro Permanent Magnet Synchronous Motor," *Energies,* vol. 14, no. 14, (2021).

Pang, D. C., Shi, Z. J., Xie, P. X., Huang, H. C., and Bui, G. T., "Investigation of an Inset Micro Permanent Magnet Synchronous Motor Using Soft Magnetic Composite Material," *Energies,* vol. 13, no. 17, (2020).

Pollock, C., "Flux Switching Motors for Automotive Applications," *IEEE Transactions on Industry Applications,* vol. 42, no. 5, pp. 1177-1184, (2006).

Rana, R., Walia, R., and Murtaza, Q., "Characterization and parametric optimization of performance parameters of DLC-Coated tungsten carbide (WC) tool using TOPSIS," *Coatings,* vol. 11, no. 7, p. 760, (2021).

Reichert, J. W. K. a. T. N. T., "Stator Tooth Design Study for Bearingless Exterior Rotor PMSM," IEEE Transactions on Industry Applications, Vol. 49, No.4, pp. 1515-1522 (2013).

Sulaiman, E., Kosaka, T., and Matsui, N., "High power density design of 6-slot–8-pole hybrid excitation flux switching machine for hybrid electric vehicles," IEEE Transactions on Magnetics, vol. 47, no. 10, pp. 4453-4456 (2011).

Tran, Q. P., Le, T. D. M., and Huang, S. C., "Multi-objective optimization of carbon fiber–reinforced polymer drilling process based on grey fuzzy reasoning grade analysis," *The International Journal of Advanced*

Manufacturing Technology, vol. 115, pp. 503-513, (2021).

Trung, D. D., Thien, N., and Nguyen, N. T., "Application of TOPSIS method in multi-objective optimization of the grinding process using a segmented grinding wheel," *Tribology in Industry,* vol. 43, no. 1, p. 12, (2021).

Vahdani, B., Mousavi, S. M., and Moghaddam, R. T., "Group decision making based on novel fuzzy modified TOPSIS method," *Applied Mathematical Modelling*, vol. 35, no. 9, pp. 4257-4269, (2011).

Walter, C. S., Polinder, H., Ferreira, J., Jänker, P., and Hofmann, M., "Torque enhanced flux-switching PM machine for aerospace applications," IEEE 20th International Conference on Electrical Machines, pp. 2585-2595 (2016).

Wang, A., Jia, Y., and Soong, W., "Comparison of five topologies for an interior permanent-magnet machine for a hybrid electric vehicle," IEEE Transactions on Magnetics, vol. 47, no. 10, pp. 3606-3609 (2011)

Wen, K.-L., Chang, T. C., and You, M., L., "The grey entropy and its application in weighting analysis," in *SMC'98 Conference Proceedings. 1998 IEEE International Conference on Systems, Man, and Cybernetics (Cat. No. 98CH36218)*, vol. 2, pp. 1842-1844, (1998).

Xiang, Z., Zhu, X., Quan, L., Du, Y., Zhang, C., and Fan, D., "Multilevel Design Optimization and Operation of a Brushless Double Mechanical Port Flux Switching Permanent Magnet Motor," *IEEE Transactions on Industrial Electronics,* vol. 63, no. 10, pp. 6042-6054, (2016).

Yang, Y., Wang, X., Zhang, R., Ding, T., and Tang, R., "The optimization of pole arc coefficient to reduce cogging torque in surface-mounted permanent magnet motors," IEEE Transactions on Magnetics, vol. 42, no. 4, pp. 1135-1138, (2006).

Zhang, J., Wang H., Chen, L., Tan, C., and Wang, Y., "Multi-Objective Optimal Design of Bearingless Switched Reluctance Motor Based on Multi-Objective Genetic Particle Swarm Optimizer," *IEEE Transactions on Magnetics,* vol. 54, no. 1, pp. 1-13, (2018).

Zhang, K., Zhan, J., and Yao, Y., "TOPSIS method based on a fuzzy covering approximation space: An application to biological nano-materials selection," *Information Sciences,* vol. 502, pp. 297-329, (2019).

Zhu, Z., and Howe, D., "Influence of design parameters on cogging torque in permanent magnet machines," IEEE Transactions on Energy Conversion, vol. 15, no. 4, pp. 407-412 (2000).

使用多變量優化法進行微型磁通開關馬達的轉子優化設計

阮登科, 黃華志, 黎氏艷媚
國立高雄科技大學機械工程學系

摘要

磁通開關馬達 (FSM) 廣泛應用於各種工業和民用領域。馬達性能的提高與平均轉矩(T_{avg})的增加直接相關,而轉矩漣波(T_{ripple})的增加則會導致不穩定性的增加,在高速運轉時尤為明顯。為了減輕這些因素對微型 FSM 運行的影響,本研究藉由 JMAG 軟體使用有限元分析方法進行了FSM馬達建模與模擬,分析了轉子幾何設計參數對馬達模型的性能影響。利用熵法確定了各項指標的加權係數。隨後,採用基於 TOPSIS 的灰色關係等級(GrG-TOPSIS)綜合評價方法,實施了多目標優化方法。這種方法旨在實現工藝設計參數的優化組合。這種創新的組合方法首次應用於 FSM 轉子設計。實驗結果顯示,最佳平均扭矩和扭矩漣波變數分別為 368.67μNm 和 16.58%,結果一致。初始參數和最佳參數之間的馬達性能之比較分析顯示,平均扭矩大小提高了 2.95%,扭矩漣波降低了 7.96%。